We are IntechOpen, the world's leading publisher of Open Access books Built by scientists, for scientists

6,900
Open access books available

185,000
International authors and editors

200M
Downloads

Our authors are among the

154
Countries delivered to

TOP 1%
most cited scientists

12.2%
Contributors from top 500 universities



WEB OF SCIENCE™

Selection of our books indexed in the Book Citation Index in Web of Science™ Core Collection (BKCI)

Interested in publishing with us?
Contact book.department@intechopen.com

Numbers displayed above are based on latest data collected.
For more information visit www.intechopen.com



3

Applications of the Parallel-LN-FDTD Method for Calculating Transient EM Field in Complex Power Systems

Rodrigo M. S. de Oliveira, Reinaldo C. Leite, Ricardo H. Chamié Filho, Yuri C. Salame and Carlos Leonidas S.S. Sobrinho
Federal University of Pará (UFPA), Centrais Elétricas do Norte do Brasil S/A (Eletronorte)
Brazil

Abstract

The present work shows the results of a R&D project carried out by ELETRONORTE and by the Federal University of Pará (UFPA). Its core objective is the development of a computational system, called LANE-MAXWELL, for performing analysis and synthesis involving electromagnetic interference (EMI) in a power system substation environment. For the analysis stage, the numerical solution of the problem is obtained by numerically solving the Maxwell's equations written in a local non-orthogonal coordinate system by employing the Non-orthogonal Curvilinear Finite-Difference Time-Domain Method (LN-FDTD). The truncation of the analysis region is done by a new formulation called LN-UPML which involves the solution of the Maxwell Equations for lossy anisotropic media in a general coordinate system. For the synthesis stage, techniques such as neural networks, genetic algorithms and particle swarm optimization are used. The computational environment conceived has a friendly data input/output interface for the user, which permits a better understanding of the electromagnetic phenomena involved. For illustrate the versatility of the computational environment some practical applications involving complex power systems structures are presented.

Keywords
Complex Power Systems Structures, Parallel Computational Environment, LN-FDTD method, LN-UPML technique.

1. Introduction

It is widely known that the Finite-Difference Time-Domain (FDTD) method is adequate for solving numerically Maxwell's Equations in order to obtain accurate transient solutions regarding lighting discharges occurring in the vicinity or on power systems (Tanabe, 2001; Oliveira & Sobrinho 2009]. These lighting pulses can produce considerable power in bands

around frequencies much higher than 60 Hertz, what demands full-wave solutions for treating and modeling this kind of problem if high accuracy is desired for solutions. In fact, frequencies can reach dozens of megahertz. Besides that, in order to consider realistic situations, complex structures which constitute the power systems must be modeled, such as wires, dielectric materials, grounding systems (and the ground itself), transmission lines and circuit elements, which are distributed in the tridimensional space in highly complex geometric arranges, such as it happens in a power substation.

This way, a computational tool was built in order to allow the modeling and simulation of such electromagnetic environments. The software, based on the FDTD method, was implemented in such way that coordinates and electromagnetic parameters of the objects are defined by the user as input data, and an equivalent electromagnetic scenario is graphically displayed as an interactive tridimensional representation. The same data is treated by the FDTD simulator, which automatically divide the analysis domain among several computers connected as a Beowulf cluster (a distributed memory computer system). This way, problems in electrodynamics are treated in a friendly way so that the users do not need to have a strong background on physics or mathematics involved in order to construct the structures to be simulated. It is also important to mention that this tool also reduces the possibility of human mistakes while modeling the scenarios, because geometric information is represented graphically.

In order to show the simulations possibilities provided by this computational approach, the following problems were simulated: 1) lightning discharge in a curved grounding system; 2) lightning discharge in a grounded transmission line tower, in which voltages and currents across its insulators were calculated; 3) transient analysis of induced voltages in transmission lines in an urban environment, in which buildings, transmission lines, grounding systems and a radio base station are considered and 4) analysis of a power system substation behavior during an atmospheric discharge, in which high-voltage switches, circuit breakers, isolators, protection inductances, lightning arresters, protection fences, grit layer, etc are some of the elements considered in the numerical model.

The obtained results were consistent with those available in the literature (for simpler cases) and with the physics related to the problems. It is worth to say that the developed methodology can be used not only on power systems problems, but it can also solve a great range of different applications related to electromagnetic transient analysis, as it is based on full-wave solutions of Maxwell's equations and on automated parallel processing. The developed software represents considerable advance in this study field, as very complex problems can now be solved.

The computational environment conceived was called LANE MAXWELL (*Synthesis and Analysis of Grounding Systems*). The accomplishment of several tasks related to the project was possible by using the developed software. The mentioned tasks are the following:

1. Development of sensors for partial discharge (PD) detection in power system environment;
2. Characterization of EMI effects in a pilot substation defined by Eletronorte;
3. Development of practices for PD sources identification;
4. Development of practices to solve EMI problems;
5. Development of an adequate mathematical formulation for the EMI analysis, capable to provide useful information for various problems;
6. Electromagnetic Shielding projects;

7. Location of PD sources on high voltage (HV) coaxial cables from the obtained transitory signals by using optimization techniques.

The necessity of characterization of the electromagnetic phenomena with a greater accuracy led ELETRONORTE to establish an R&D project in cooperation with UFPA (Federal University of Para). This level of accuracy makes the analysis and synthesis of the problems more complex making it unviable by analytic means, in such way the numerical solution techniques became the most adequate choice for the treatment of practical problems. Nowadays, numerical solutions are considered to be as important as experimental measurements, as long as they are complementary to each other. The main objective is to make the practical measurements to have a more economic and safer implementation and procedures.

In this context, this work contributes in several ways, based on the development of a computational environment that permits the realization of the analysis and synthesis of problems in electrodynamics in a friendly way. The methodology used in the analyses involves the solution of the Maxwell's equations in Time Domain, written in curvilinear coordinates, by the Finite-Difference Time-Domain method (Taflove & Hagness, 2005). The analysis scenarios are truncated by the uniaxial perfect matching layer technique (UPML): a specific mathematic formalism had to be developed in order to adequate this technique to the curvilinear system (Oliveira & Sobrinho, 2007); for the synthesis several optimization techniques are available, such as: genetic algorithm (Rahmat-Sami & Michielsssen, 1999), particle swarm optimization (Lazinica, 2009) and artificial neural networks (Hagan, & Menhaj, 1994). The software is complemented by input/output interfaces that facilitate the creation of scenarios, visualization of electromagnetic field distribution, video generation, visualization of scenarios, generation of voltage and current graphics, etc.

2. Related Theory

A. The General Coordinate System

Considering a general or curvilinear coordinate system, a position vector $\vec{r}$ can be obtained as a function of the general coordinates, and its differential length vector $d\vec{r}$ is given by

$$d\vec{r} = \sum_{l=1}^{3} \frac{\partial \vec{r}}{\partial u^l} du^l = \sum_{l=1}^{3} \vec{a}_l \, du^l, \tag{1}$$

in which the vectors $\vec{a}_l$ are called unit vectors and form a unit base; which defines the axes of a general curvilinear space (each point in space has its own coordinate system). Figure 1 shows the vectors $\vec{a}_l$ (l = 1, 2, 3) which are tangent to the u^l axes and can be written as functions of the Cartesian Coordinates: x, y and z. An alternative set of three complementary vectors $\vec{a}^l$, reciprocal vectors, can be defined in such a way that each one is normal to two unit vectors with different indexes, forming a reciprocal base. This set can be mathematically calculated by the expressions

$$a^1 = \frac{\vec{a}_2 \times \vec{a}_3}{\sqrt{g}}, a^2 = \frac{\vec{a}_1 \times \vec{a}_3}{\sqrt{g}}, a^3 = \frac{\vec{a}_1 \times \vec{a}_2}{\sqrt{g}}, \tag{2}$$

in which $\sqrt{g}$ is the volume of the hexahedra formed by the vectors $\vec{a}_1, \vec{a}_2, \vec{a}_3$ (Fig.1). In (2), $\sqrt{g} = \vec{a}_1 \cdot (\vec{a}_2 \times \vec{a}_3)$, in which g is the determinant of the metric matrix or the covariant tensor (Taflove & Hagness, 2005).

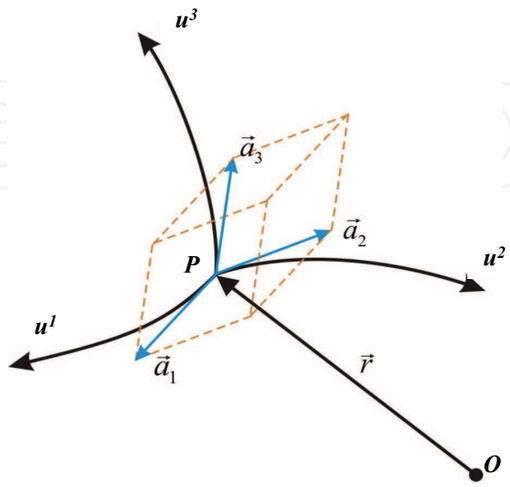


Fig. 1. Curvilinear coordinate system at point P and the unit vectors in a non-orthogonal cell.

Based on the previously presented idea, let a fixed vector $\vec{F}$ to be represented by the unit system or by the reciprocal system as shown by (3)

$$\vec{F} = \sum_{l=1}^{3} f^l \cdot \vec{a}_l = \sum_{l=1}^{3} f_l \cdot \vec{a}^l . \tag{3}$$

In (3), f_l and f^l are called covariant and contravariant components of the vector $\vec{F}$, respectively. The components f^l and f_l can be calculated by means of the dot product of the previous equation by $\vec{a}^l$ and $\vec{a}_l$ respectively, as it is shown by (4).

$$f^l = \vec{F} \cdot \vec{a}^l, f_l = \vec{F} \cdot \vec{a}_l . \tag{4}$$

These components (covariant and contravariant) can be related by means of the following expressions:

$$f_m = \sum_{l=1}^{3} g_{lm} \cdot f^l, f^m = \sum_{l=1}^{3} g^{lm} \cdot f^l . \tag{5}$$

It is worth mentioning that the unit and reciprocal vectors do not necessarily have unitary amplitudes because they depend on the nature of the curvilinear coordinate system used (cells' edge lengths). Hexahedrons similar to that in Fig. 1 are used as Yee's cells. This way,

the appropriate set of unit vectors and their respective unitary lengths are defined by the elementary equations

$$\vec{i}_1 = \frac{\vec{a}_1}{\sqrt{\vec{a}_1 \cdot \vec{a}_1}} = \frac{\vec{a}_1}{\sqrt{g_{11}}}, \vec{i}_2 = \frac{\vec{a}_2}{\sqrt{g_{22}}}, \vec{i}_3 = \frac{\vec{a}_3}{\sqrt{g_{33}}}. \tag{6}$$

From (3), we can write

$$\vec{F} = F^1\vec{i}_1 + F^2\vec{i}_2 + F^3\vec{i}_3, \tag{7}$$

in which F^l represents the physical components in the base system and their values are thus calculated by (8)

$$F^l = f^l \cdot \sqrt{g_{ll}}, F_l = \sqrt{g^{ll}}. \tag{8}$$

This representation of vectors can be used to describe electric and magnetic fields' components, as shown in the next topic.

B. The LN-FDTD Method applied for solving Maxwell's Equations

The Maxwell's equations in differential form can be written for lossy, isotropic, non-dispersive media as:

$$\nabla \times \vec{E} = -\mu \frac{\partial \vec{H}}{\partial t} \quad and \quad \nabla \times \vec{H} = \sigma \vec{E} + \varepsilon \frac{\partial \vec{E}}{\partial t}, \tag{9}$$

in which $\vec{E}$ is the electric field strength vector, $\vec{H}$ is the magnetic field strength vector, ε is the electrical permittivity of the media, μ is the magnetic permeability of the media and σ is the electrical conductivity. By calculating the contravariant components of the fields $\vec{E}$ and $\vec{H}$, by using central differences approximations for the derivative terms and by observing the primary and secondary cells in Fig. 2, the equations, for updating the components of the fields, can be obtained as follows:

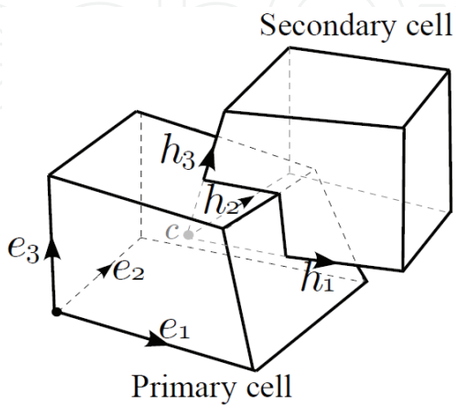


Fig. 2. Distribution of the covariant components in Yee non-orthogonal cells: primary cell for the electric field and secondary cell for the magnetic field.

For obtaining a field component (for example, the first contravariant component of $\vec{H}$, h^1), (4) (and (2)) can be used for l=1. In this case, the dot product operation is performed on Faraday's law. That is

$$\left(\nabla \times \vec{E}\right).(\vec{a}_2 \times \vec{a}_3)/\sqrt{g} = -\mu\left(\frac{\partial \vec{H}}{\partial t}\right).\vec{a}_1, \tag{10}$$

from which it is easy to see that

$$\frac{\partial H^1}{\partial t} = -\frac{1}{\mu\sqrt{g}}\left(\frac{\partial e_3}{\partial u_2} - \frac{\partial e_2}{\partial u_3}\right), \tag{11}$$

by observing that, from (2), it is possible to say that $\vec{a}^m.\vec{a}_n = \delta_{m,n}$, in which $\delta_{m,n}$ is the Konecker delta function. Equation (11) and the equations for the other five field components can be represented by finite differences by using the standard Yee's algorithm.

C. Stability and Precision of the LN-FDTD Method

The numerical stability of the method is related to the increment Δt, which follows the condition stated by (12),

$$\Delta t \leq \frac{1}{c \cdot \max\left(\sqrt{\sum_{l=1}^{3}\sum_{m=1}^{3} g^{lm}}\right)}. \tag{12}$$

To reduce the effects of numerical dispersion to adequate levels and in order to ensure the precision of the calculations, the dimensions of each non-orthogonal cell in every direction should be less than λ/10 (Taflove & Hagness, 2005), where λ is the smaller wavelength involved in the problem.

D. UPML for Conductive Media – Truncation of the LN-FDTD Method

The Maxwell's equations in frequency domain for an unaxial anisotropic media, can be written as follows:

$$\nabla \times \vec{E}^* = -j\varpi\mu_0\mu_r\bar{\bar{S}}\vec{H}^* \quad and \quad \nabla \times \vec{H}^* = (j\varpi\varepsilon_0\varepsilon_r + \sigma)\bar{\bar{S}}\vec{E}^*, \tag{13}$$

in which ω defines the angular frequency of the electromagnetic wave; $\vec{E}^*$ and $\vec{H}^*$ are the Fourier transforms of the electric field strength and magnetic field strength, respectively, μ_r is the relative magnetic permeability and ε_r is the relative electrical permittivity, $\bar{\bar{S}}$ is the tensor that promotes the attenuation along the coordinate axes normal to the layers of the absorbing region and σ is the media conductivity. $\bar{\bar{S}}$ has the following form

$$\overline{\overline{S}} = \begin{bmatrix} \frac{S_2 \cdot S_3}{S_1} & 0 & 0 \\ 0 & \frac{S_1 \cdot S_3}{S_2} & 0 \\ 0 & 0 & \frac{S_1 \cdot S_2}{S_3} \end{bmatrix}, \tag{14}$$

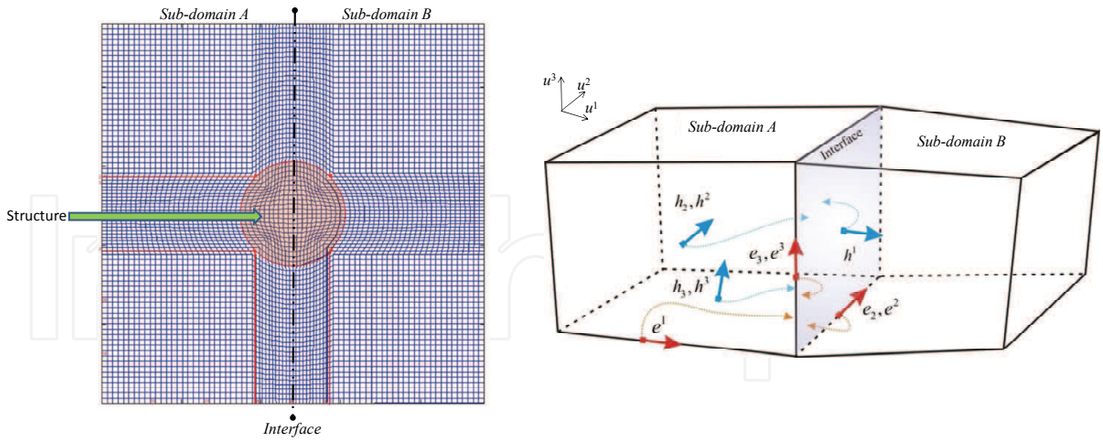
where S_α (α=1, 2, 3) are the parameters that characterize the UPML attenuation along the mentioned general coordinate axes, for which they assume the form (Taflove & Hagness, 2005):

$$S_\alpha = K_\alpha + \frac{\sigma_\alpha}{j\varpi\varepsilon_0}. \tag{15}$$

By following the procedures similarly to that was indicated in item B (and by introducing auxiliary variables for calculating transformations of fields to time domain), the updating equations for the field components are obtained (Oliveira & Sobrinho, 2007).

E. Parallel Processing for the LN-FDTD Method

The main idea of using parallel computation for solving electromagnetic problems by the LN-FDTD is based in a division of the analysis domain into sub-domains A and B (Fig. 3a). Each sub-domain is a fraction of the whole numerical volume that will be treated by a single processing core. Each core executes essentially the same FDTD code, but with particular boundary conditions. Field information must be exchanged at the sub-domains' interfaces, as illustrated by Fig. 3b.



(a) (b)

Fig. 3. (a) Domain decomposition into two sub-domains and cross section of a 3-D non-orthogonal grid; (b) the field components exchanged between two neighbor sub-domains.

As it is also illustrated by Fig. 3(a), some structures can be divided among two (or possibly more) sub-domains. This issue was treated by implementing a subroutine, which automatically distributes the media parameters among the processing units in such way that

the electromagnetic behavior of the divided scenario is identical to the behavior of the full numerical domain processed by a single core. This way, the software can generate complex electromagnetic scenarios by automatically defining the parameters for each CPU by using the data defined by the user in a graphical user interface (GUI), which is graphically displayed by a specific visualization tool developed by using the OpenGL library. This tool, associated to the automatic domain division subroutine, significantly reduces the probability of human errors when constructing and simulating the scenarios. Many figures on this work are direct outputs of the 3D-viewer.
The developed software also supports the insertion of thin-wires (Baba et al., 2005) and thin-planes (Maloney & Smith, 1992) (considering the Cartesian coordinate system), and ground ionization due lighting discharges (Ala et al., 2008).

3. Software Applications

This section, results obtained by using the developed computational environment are presented. Such applications range from the analysis of simple grounding systems to highly complex electromagnetic structures, such as the analysis of the effects of lighting surges on power substations. This way, initially a validation of the implementation is shown, by comparing experimental and numerical results for a grounding structure. Then the importance of using the local coordinate system is evidenced for a grounding structure which geometry is not compatible to the Cartesian system of coordinates. Finally, the effects of lighting currents on three complexes are analyzed for three cases: transmission tower, induced voltages on transmission lines for an urban block of buildings and for the structural part of a power substation.

A. Analysis of a rectangular grounding system.
In order to validate the implementation of the parallel numerical algorithm previously described, the transient responses of a rectangular electrode due the application of a artificial lighting current, originally proposed and analyzed by (Tanabe, 2001) were calculated. The geometry is illustrated by Fig. 4, which was reproduced in the computational environment.
Basically, this problem consists on a rectangular grounding electrode, with dimensions of 0.5×0.5×3.0 m, buried in a soil with electromagnetic parameters σ = 2.28 mS/m, $\mu = \mu_0$ and $\varepsilon = 50\ \varepsilon_0$. Additionally, the problem includes two circuits: one for current injection and other for voltage measurement, which dimensions are defined by Fig. 4. This figure also shows the identification of the sub-domains assigned to each processing core of a Beowulf cluster of PCs (regions numbered from 1 to 10), defined automatically by the automatic domain division subroutine.
Fig. 5 shows the numerical results obtained by the simulator developed in this work and the results obtained in (Tanabe, 2001) by conducting physical experiments. It is possible to observe that experimental and numerical transient responses for current, voltage (and consequently for the Voltage/Current ratio) are agreeing for most of the time. The main propose of this test is to certify that the parallel simulator generates trustable and accurate results.

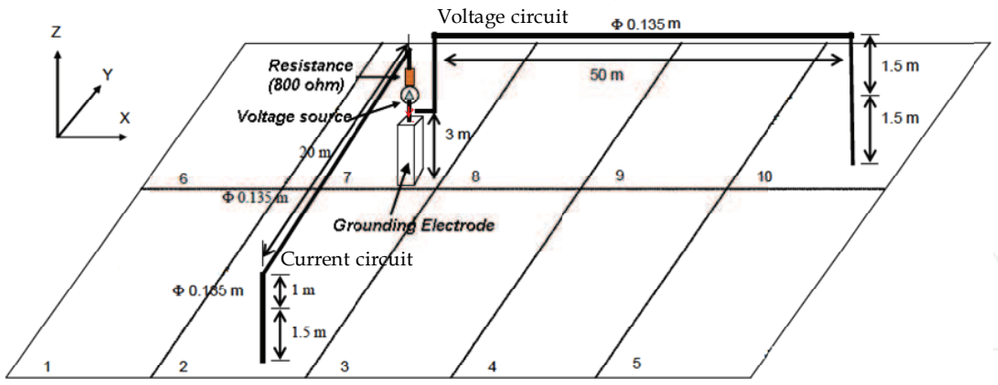


Fig. 4. Representation of the grounding electrode and of the measuring system originally proposed and analyzed by (Tanabe, 2001) and the automatic domain division schema defined automatically for this problem.

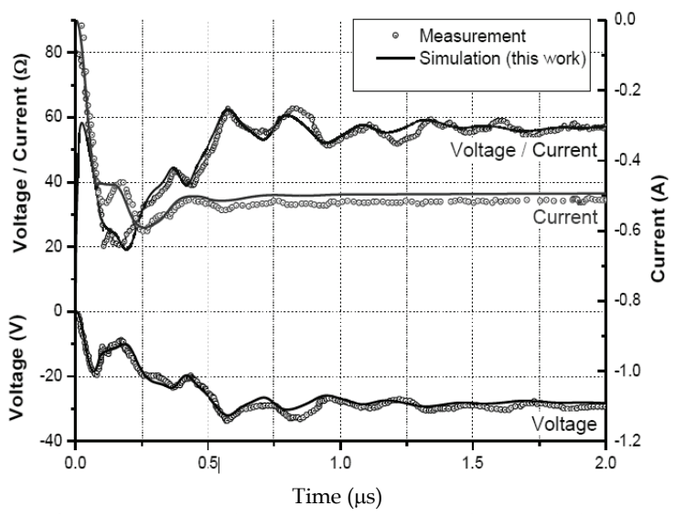


Fig. 5. Comparison of experimental measurements obtained by (Tanabe, 2001) to the numerical results obtained in this work.

B. Simulation of a circular grounding system by using Cartesian and curvilinear coordinates.

Figure 6 shows four vertical grounding rods connected by a circular conducting ring, modeled by the classical FDTD formulation. The rods are four meter long and the ring's diameter is eight meters, which is positioned 0.5 m under the ground surface The soil electrical parameters are $\sigma = 2$ mS/m and $\varepsilon = 50\ \varepsilon_0$. The idea is to compare results generated by employing the classical (orthogonal) FDTD method and the curvilinear FDTD methodology (LN-FDTD) and to investigate the influence of the staircase approximation effects for non-rectangular grounding structures and to evidence the need for using non-orthogonal modeling for such cases. The computational mesh illustrated by Fig. 3a was used for simulating this structure by using the LN-FDTD method. The circumference defined by the mesh of Fig. 3a was used to represent, in a more accurate way, the metallic grounding ring analyzed in this example.

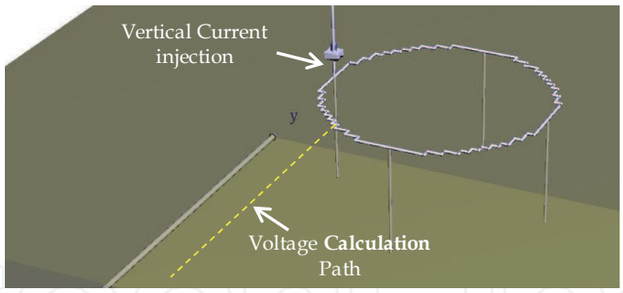


Fig. 6. A circular grounding structure modeled by using the Cartesian coordinate system.

According to (Mattos, 2004), the influence of the diameter of the conductors is negligible for the steady grounding resistance R (0.0 Hz), which is given by the equation

$$R = \left(\frac{1}{4L} + \frac{1}{4\pi D}\right)/\sigma \, . \tag{15}$$

In (15), L is the rods' length and D is the diameter of the considered circumference. For this case, the expression (15) provides R = 36.224 Ω, which agrees very well to the result obtained by using the LN-FDTD method (Fig. 7) at 2.5 μs (R = 36.973). This Figure also presents the results obtained for simulations performed by the classical FDTD algorithm, by approximating the conducting circumference by staircase. It is observed that, as the FDTD spatial step Δ is reduced, the results tend to converge to the result obtained by the LN-FDTD method (for both, the steady state and transient periods). In Fig. 7, it is also possible to observe that the ohmic values calculated by the FDTD method are higher than the values obtained by the LN-FDTD simulator. This is consistent, as the stair case approximation for the circular path for the electrical current acts as an obstruction for the movement of the electrical charges, thus increasing the voltage/current ratio. This effect is greatly reduced by the non-orthogonal coordinate system and it clearly shows that there is the necessity of avoiding this kind of geometric approximation for performing such analysis especially for higher frequencies.

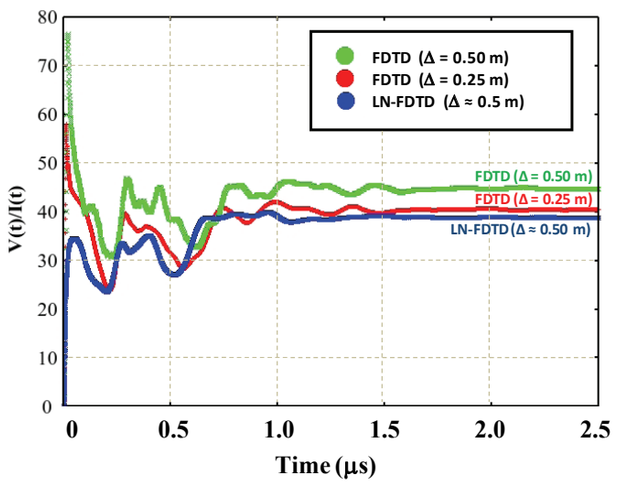
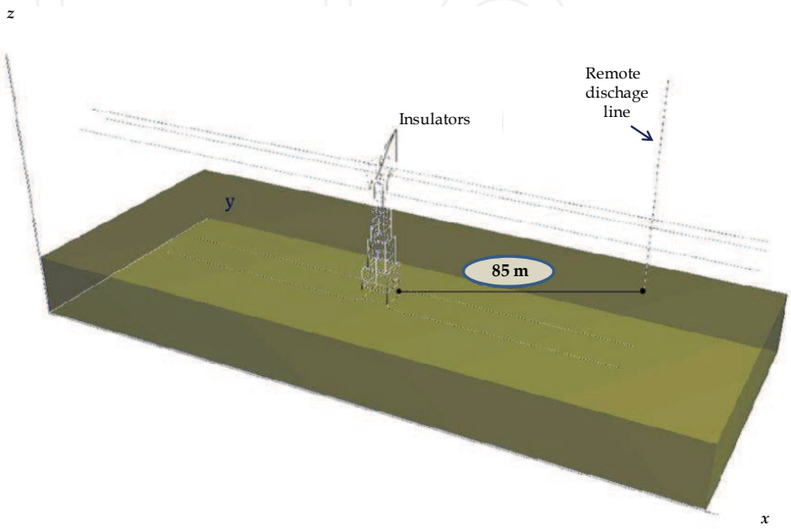


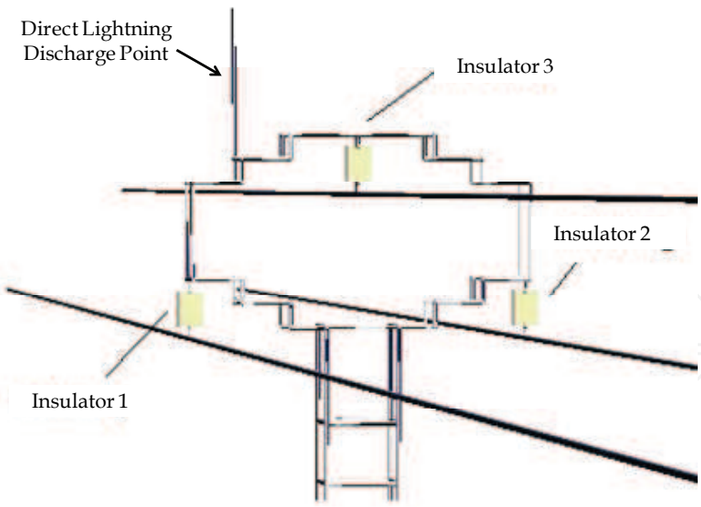
Fig. 7. Voltage / Current ratios obtained by using the FDTD method (Δ = 0.50 m and Δ = 0.25 m) and by the LN-FDTD method (Δ around 0.50 m).

C. Transmission Line Tower and Induced voltages on Line Insulators due to Remote Lighting Discharge

One of the several applications of the developed computational environment is the simulation of atmospheric discharges and the calculation of induced voltages at specific parts of a structure of interest. For this problem, this structure is a transmission line tower and its line insulators.



(a)



(b)

Fig 8. (a) overview of the scenario created for the calculation of the induced voltages due to atmospheric discharges and (b) detail of the positioning of the insulators, transmission lines and the location of the point of occurrence of the direct lighting stroke.

Fig. 8 shows the simulation scenario created. The goal here is to calculate the transient induced voltages at the insulators due to a lighting current reaching the ground surface 85

meters away from the tower. The simulations were carried out by considering the following parameters: numerical volume: 250x70x100 m by using cubic Yee cells with edges of 0.5 m; ground parameters: $\varepsilon = 50\ \varepsilon 0$ and $\sigma = 2$ mS/m; insulator parameters: the insulator modeled has 1.0 m of height with the electrical conductivity of 10^{-11} S/m and relative electrical permittivity of 7.5; excitation source: the same used previously (Tanabe, 2001). The lighting discharge was included into the analysis domain by creating a vertical conductor, which penetrates the field absorbing boundary region (UPML) at its top (with impedance matching), representing an infinitely long conductor. By forcing the magnetic field around this conductor to follow the function defined by (Tanabe, 2001), a punctual transient current (52 meters from ground surface) with maximum value of 10 kA was created and used as source. The transmission lines and the grounding rods also penetrate the UPML region.
The basis of insulators 1 and 2 (Fig. 8b) were placed at 43.5 meters from the ground surface and the basis of insulator 3 was placed 49.5 meters from the ground plane. It was also simulated the case in which the lighting current occurs at the tower structure, at the point indicated by Fig. 8b and the obtained results for induced voltage on insulator 1 are compared in Fig. 9.
Fig. 9 shows the behavior of the voltage induced on the insulator 1 (*z*-oriented path). In Figure 19, it is shown the induced voltage during the transient period and in Figure 19b it is shown the induced voltage for the stationary period. For this insulator, induced voltage reaches no more than 450 kV during the transient time evolution. As expected, by considering the direct lightning current injection at the tower top, produces a much higher peak, which reaches approximately 1.8 MV at 0.5 μs, as shown by Fig. 9a. As shown by Fig. 9b, the difference between the steady induced voltages is approximately 24 kV. For each 10 kA of lighting current peak, the insulator can be subjected to 50 kV (which is added to the nominal line voltage) during considerable amounts of time.

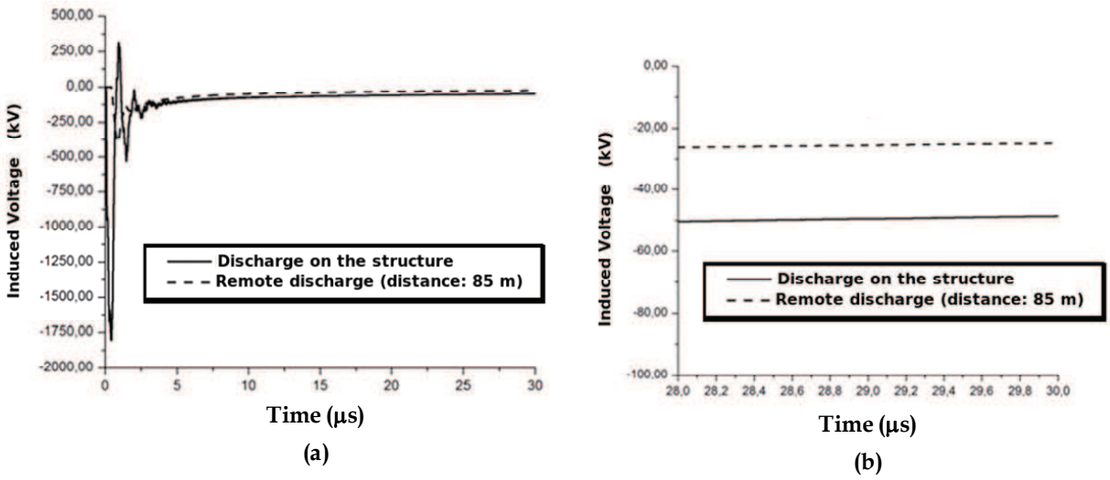


Fig. 9. (a) induced transient voltages and (b) the induced voltages at the stationary period

D. Distribution Line in Urban Environment: lighting discharge at a Radio Base Station (RBS).

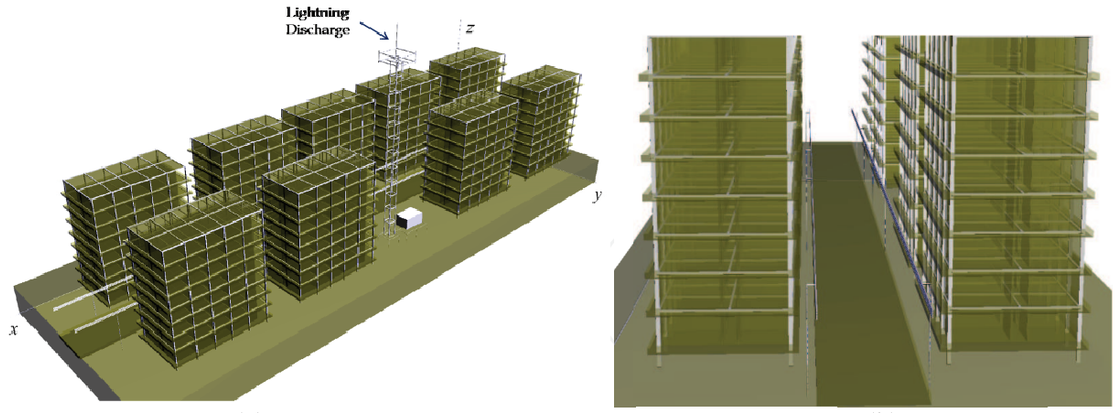
In recent years, due to world-wide expansion of cell phone systems in urban areas, the raising of tower-like structures operating as radio-base stations (RBSs) became common in

cities. With considerable heights, around 50 meters, these structures are preferential points for atmospheric discharge strokes. The discharges can occur at the tower's lightning rod or at its metallic body. The occurrences of discharges on telephone towers cause an undesirable set of effects, either in the ground (such as increase of potentials and return currents in grounding systems) or at lines for energy transmission (causing outbreaks due to electromagnetic induction). Such outbreaks are characterized by high-voltage peaks, followed by sudden potential differences between pairs of conductors of the low voltage lines, affecting the consumer units with possible serious damage to electric and electronic devices.

The goal of this application of the LANE-MAXWELL software is to study the induced voltages on low-voltage systems and to estimate how the electromagnetic field, generated by atmospheric discharges on high metallic structures might behave by taking into account the complex structures with different materials around the transmission lines. The two low voltage lines in this scenario can be represented by four metallic cables suspended in the air lined up and separated vertically by a specific distance. On both modeled low voltage lines, two connections between the neutral cable and the ground are established. These low voltage cables were positioned in such a way that their extremities penetrate the UPML of the analyzed region. This set of complex structures modeled in this simulation is represented by a realistic Radio Base Station with its metallic container of equipments and its grounding structure, a set of realistic modeled buildings located next to the RBS, and a realistic road, which was positioned parallel to the *x* direction of the analysis region as shown by Fig 10. The conception of a scenario was carried out by using the following parameters:

1. Nine eight-floor buildings of 24 m height each, with the following dimensions: 24x12.8x24 m;
2. Analysis region with 168x60x64 m;
3. Yee cells with edges measuring Δ = 0.2 m (840x300x320 cells);
4. Lateral and frontal separation spaces for Buildings: 6 m and 14 m, respectively;
5. The bars were considered as perfect metal conductors;
6. Wall and street material: reinforced concrete (σ=0.2 S/m, ε_r = 7.5 and μ_r = 1);
7. Low voltage lines with three cables as phase and one as neutral conductors, located at 10 m and 20 m away from the geometric center of a cell phone radio base station (RBS);
8. Cable heights of 6.6 m, 6.8 m, 7.0 m (the three phase lines) and 7.2 m (the neutral line) respectively from the ground. Cables' diameter: 15 mm.
9. RBS is 50.0.m-high and the container has dimensions of 6.0x4.0x3.0 m ;
10. Neutral grounding with ½"x 3 m length cooper rods, with a grounding resistance of 80 Ω.
11. Conductive earth with electrical parameters σ= 0.0040836 S/m and ε_r = 10.
12. Excitation source: see Fig. 12a.

Figure 11 shows the scenario built in the LANE-MAXWELL environment, detailing the above specifications.



(a) (b)

Fig. 10. (a) the virtual urban environment built for analysis of the electromagnetic induced voltage on electrical distribution lines (b) a longitudinal view of the street and distribution line.

The obtained transient induced voltages on the cables due to an atmospheric discharge on the RBS (Fig. 12a) are shown by Figure 12b. In this case, the ground system of the buildings and the line were not connected together trough wires (current flows trough ground only). Fig. 12b shows that, for the three live cables located 10 meters away from the tower, the peak value of the induced voltage is around 8.0 kV when the simulation time is about 1.2 μs. The induced voltages on both energy lines are caused partially by the electric current that propagates trough ground and circulates trough the lines' grounding electrodes and partially by the direct and indirect incidences of the electric field on the lines. It is important to mention that the smooth oscillations present on Fig. 12b can be caused by reflections of this propagating electromagnetic field on the buildings' walls, on the ground surface and on the lines themselves, and these oscillations tend to disappear as time progresses.
Moreover, results show that induced voltage at a line takes more than a half microsecond to start decaying from its maximum value. However, it is important to mention that the voltage induced at the neutral cable was also increased proportionally, so that the live-live and live-neutral voltages did not suffer any major changes. In the final moments of the simulation, all four curves tend to get closer quickly. Similar behavior is observed for the line located 20 m away from the tower.
Figure 13 shows the electric field spatial distributions and its time evolution at the ground surface (Figs. 13a-c) and at the vertical *yz*-plane which contains the current source (Figs. 13 d-e).
In order to facilitate the visualization of the electric field distribution inside the analysis region, the behavior of the electric field was registered at two planes inside the structure, generating hi-resolution colored images, in which the blue tones represent lower values of electric field, and the red tones or represent higher intensities of electric field. Fig. 13 shows the electric field distribution on the *xy* plane, with z = 7.8 m (ground surface) at three different steps of simulation. These figures show that the electric field is more intense at adjacent regions of the RBS' grounding mesh, and these values decays abruptly as the observation point departs from it, generating significant amounts of step potentials towards the mesh neighborhood. Such electric field behavior generates a potentially dangerous region near these structures during a lighting stroke. In Fig. 13, it is still possible to visualize

the *yz*-plane of the structure at x = 84 m (midpoint of the energy line) after 3 μs (12982 iterations) of simulation. It is clear that the electric field which penetrates the buildings is less intense than those present in regions outside this structure. This fact is due to the metallic and concreted constitution of the building structure, which acts as a Faraday's Cage the field, keeping most of the energy of the scattered electromagnetic wave outside the buildings' structure.

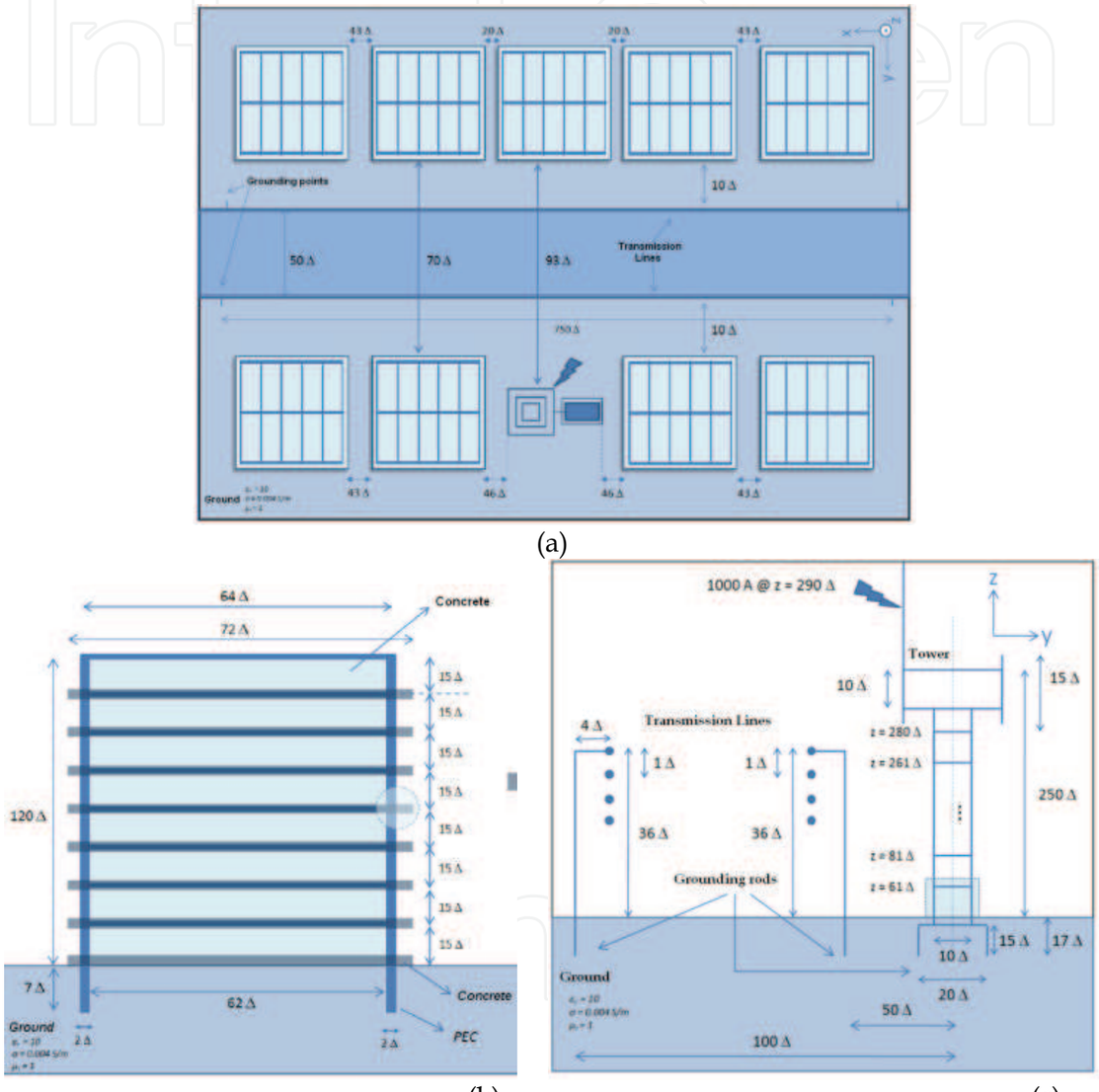


Fig. 11. (a) top overview of the urban block, (b) dimensions of one of the buildings and (c) tower, grounding system and transmission lines geometric configuration.

The analysis of the obtained results show high levels of overvoltage and potential differences between live to live and live to neutral conductors on electrical distribution systems, during lightning strokes on a RBS. The results computed with the FDTD method, include full wave solutions for complex structures, involving dielectric materials, a complex

tower model, transmission lines, grounding systems, and the consequent complex electromagnetic interactions involving surface waves, diffractions, refractions, and reflections. It has been shown that all those aspects substantially affect results, which, in this work, are close to realistic situations.

The problems observed here (relative to transitory high voltage induced in transmission lines) represent high risk when considering the final consumer unit, providing both material and human health damage.

Besides that, it was possible to verify from the electric field spatial distribution that high potential differences induced on the soil surface can be found in regions near the tower and its grounding mesh. Such structures are usually located near residences, or in places with constant circulation of people. Telecommunication towers require special attention by the operators which are responsible for the service and by the local energy company as well, keeping safe areas located near those installations, as well as the energy consumer unit.

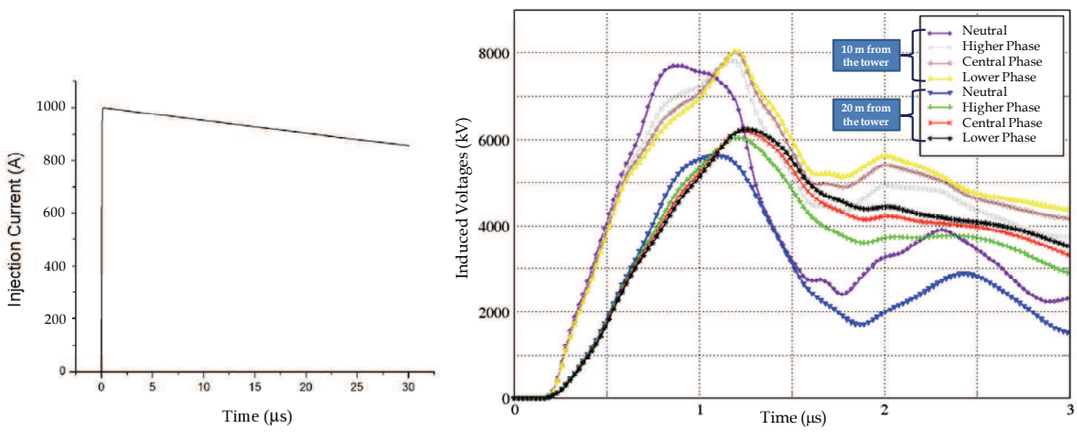


Fig. 12. (a) waveform of the injected current, used as excitation source and (b) the transient voltages obtained for each transmission line.

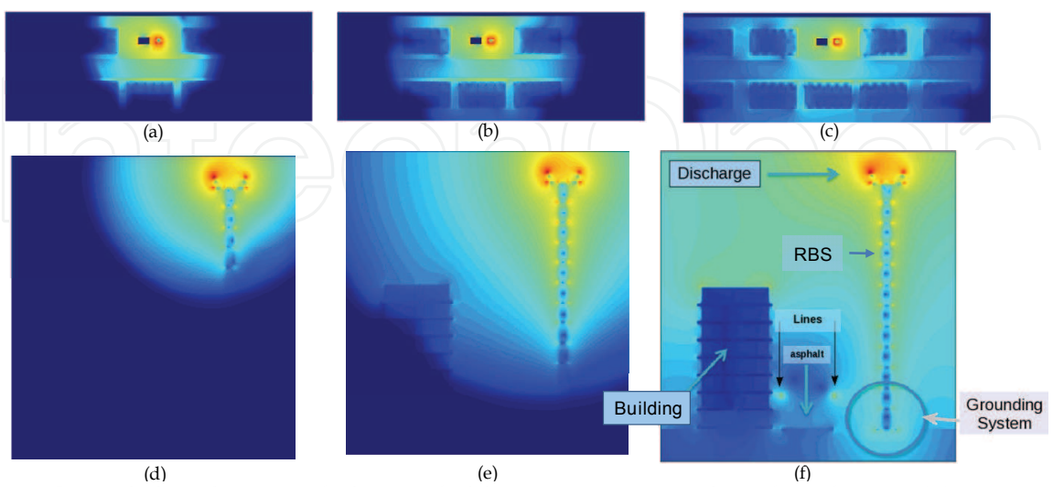


Fig. 13. Spatial distribution of electric field intensity: ground surface for t = (a) 900 Δt, (b) 1050 Δt, (c) 1440 Δt; and at the plane x = 420 (the plane containing the source) for t = (d) 330 Δt, (e) 420 Δt and (f) 1410 Δt.

E. Analysis of Induced voltages on Transmission Lines of a Power Substation due to Atmospheric Discharge.

Figure 14 shows an overview of a computational model of the power substation created by using the LANE-MAXWELL software. It is composed by the structural elements of high-voltage switches, insulators, transmission lines, towers, fence, grit layer, grounding grid, current Transformers, voltage transformers, lightning arrester, etc.

The analyzed region's volume is 1000x195x45 m^3, which is represented by cubic Yee cells with edges measuring 0.5 m. As indicated by Fig. 14, the lighting current was injected at a lighting arrester placed near the 230 kV line, with a maximum value of 1.0 kA (Tanabe, 2001). The wave propagation phenomenon was analyzed up to 12 μs after the beginning of the lighting process. The electrical parameters used for representing the ground region were $\varepsilon = 50\ \varepsilon_0$ and $\sigma = 2$ m S/m. The grit layer was modeled as an isotropic media with thickness of 0.5 m and with $\sigma = 0.333$ m S/m $\varepsilon = 50\ \varepsilon_0$. This model follows the specifications of a real substation, which is under responsibility of Eletronorte, installed at the city of Belém (Brazil).

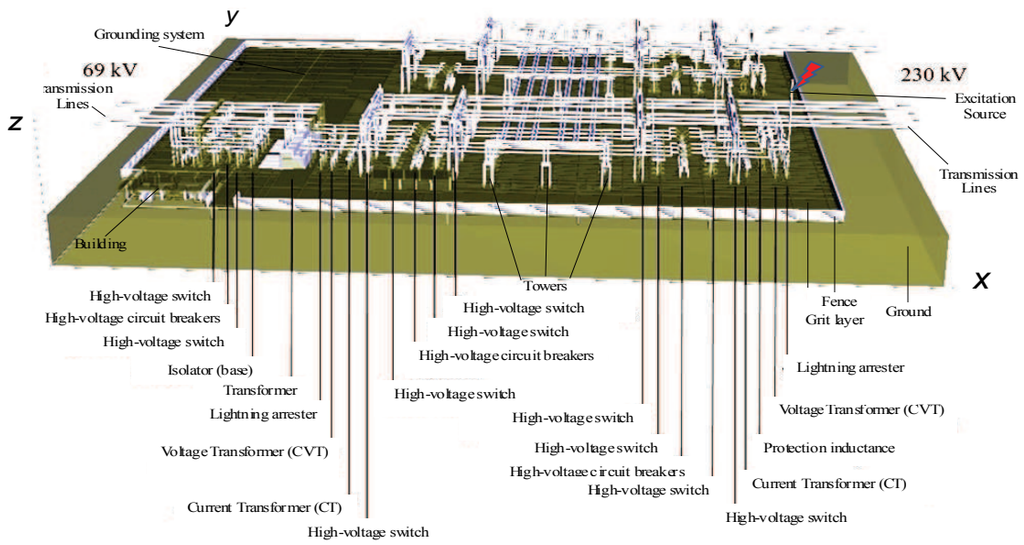
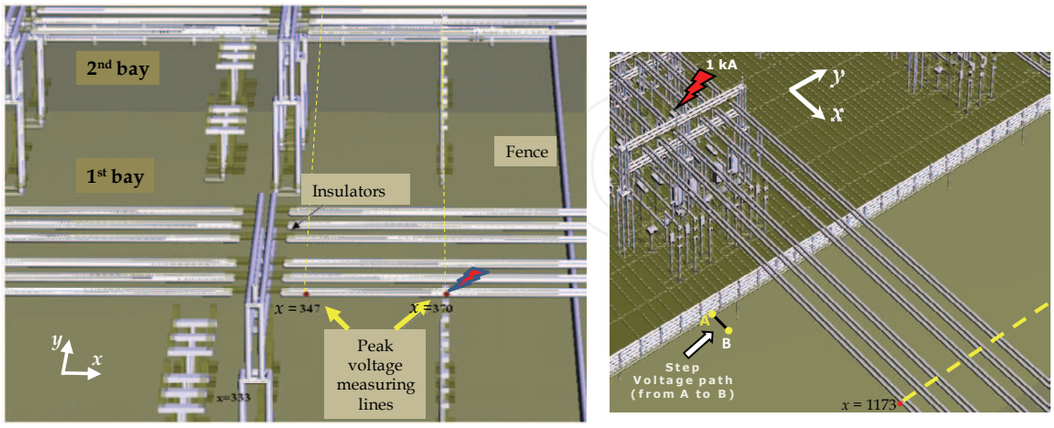


Fig. 14. Structure of the Power Substation represented in LANE-MAXWELL.

In order to create the scenario of Fig.14 with precision, specific database software has been developed. The idea is to create prototypes of the objects of the substation and to clone them at proper spatial coordinates. These objects (towers, switches, etc.) are composed by basic elements of the simulation software (metal and dielectric blocks and thin wires), which are grouped forming a prototype. A text file containing the positions of each clone of each prototype defines the electromagnetic environment. Then, the domain decomposition subroutine distributes the basic elements among the processing sub-domains, which quantity of cores to be used is defined by the user (Fig.3a). Here, sixteen 64-bits processors were used as a Beowulf cluster for solving this problem, which requires approximately 12 hours for concluding the computer simulation. Each core processed a volume of 62.5x195x45 m^3 each time step.

Figure 15a shows two *y*-aligned lines (in doted yellow style) over which induced transient voltages, calculated from the transmission lines to ground, were registered. The red points numbered as 370 and 347 indicate the discrete Yee's indexes related to the *x* direction, where the voltages are measured. Figure 15b defines of the path used for integrating electric field,

at the ground surface, in order to calculate the transient step voltage outside the substation, in the region as close as possible to the discharge point. The points A and B are separated by one meter (average separation between the legs of a human victim).



(a) (b)

Fig. 15. (a) Definition of two of the lines (dashed yellow style) were induced voltage peaks were registered. Voltages were measured from transmission lines to ground and (b) definition of the path used for integrating electric field and determining the transient step voltage (from A to B) ; definition of the line in which induced voltages were registered at the transmission lines (x = 1173). Coordinates are given in cells.

Figure 16 presents the obtained maximum induced voltages on the transmission lines, measured from the ground surface to those lines, considering (a) x = 370, (b) x = 347, (c) x = 316 and (d) x = 1173, along the y direction. The voltage values obtained for each transmission line are indicated by the black dots on the curves (lines were obtained by interpolation).

As shown by Fig. 15a, the line in which x = 370 is the closest to the discharge point. For the first line, the voltage peak induced reaches about 110 kV (Figs. 16a and 16b). For its neighbor parallel line, the induced voltage is radically reduced to 35 kV (x = 370) and to about 15 kV for x = 347. For the case of Fig. 16a, the induced voltage on the remaining transmission lines decreases exponentially, reaching about 10 kV at the second bay's lines. For the case of Fig. 16b (12 m from the line considered in Fig. 16a), it is possible to see that the decay pattern is close to an exponential function with oscillations for the first bay lines. The voltages for the second bay are also close to 10 kV for each kA injected.

Figure 16c shows similar results obtained for x = 316. It is possible to see in Fig. 15 (a) that between this point and the discharge coordinates there are several structures, like towers and switches, which act as reflective objects to the electromagnetic field, what justifies the considerable reduction of the peak voltage for the first line (to about 50 kV). The induced voltage to the neighbor line drops to 25 kV and decays almost exponentially to about 6.5 kV at the second bay. The reduction due the reflection of the fields are confirmed when results of Fig. 16d are analyzed. The reference point is x = 1173 (Fig. 15b), which is outside the substation (401 m from the discharge point). The maximum induced voltage is close to 72 kV, decreasing exponentially to 5 kV as distant lines are analyzed. It is also confirmed by analyzing Fig. 17, which shows the electric field distributions for (a) t = 0.225 μs, (b) t = 0.365

μs and (c) t = 1.00 μs. In those figures, the blue color represents small amplitudes, green represents intermediate strengths and red is associated to the regions of greater intensity for electric field. For all cases, it is possible to see that the electric field presents smaller intensities as one moves from the fist bay (where the discharge occurs) to the second bay (in y-direction). However, when one moves from the first bay to outside of the substation (in -y-direction), the field attenuation is less intense.

Fig. 18 (a) shows the obtained step voltage between the points A and B indicated at Fig. 15b. It is possible to see that after approximately 1 μs of the beginning of the lighting discharge, this voltage reaches its maximum value of about 807 V for each kA of peak current. However, its time duration is relatively short. However, the person can be exposed to voltages around 200 V for each kA of lighting current for a much longer time, depending on the time and amplitude characteristics of the injected current. Finally, Fig. 18b shows the electric field distribution at the ground grid plane after 38.5 ms of simulations, illuminating the grid. It is possible to observe that there are red dots, indicating higher intensities of the field, which are associated to the electrical connections of the substation devices to the ground grid. This indicates that current is returning or it is being injected to the grounding mesh.

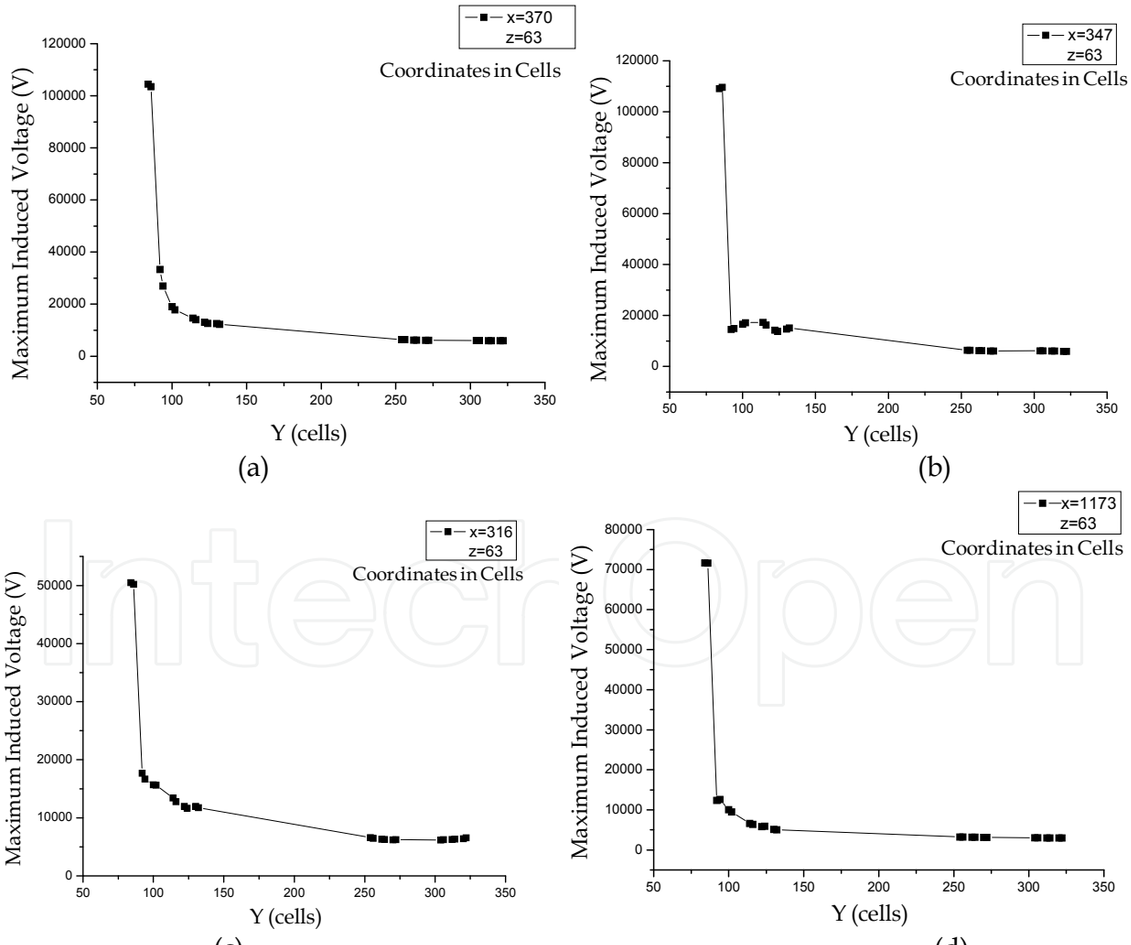
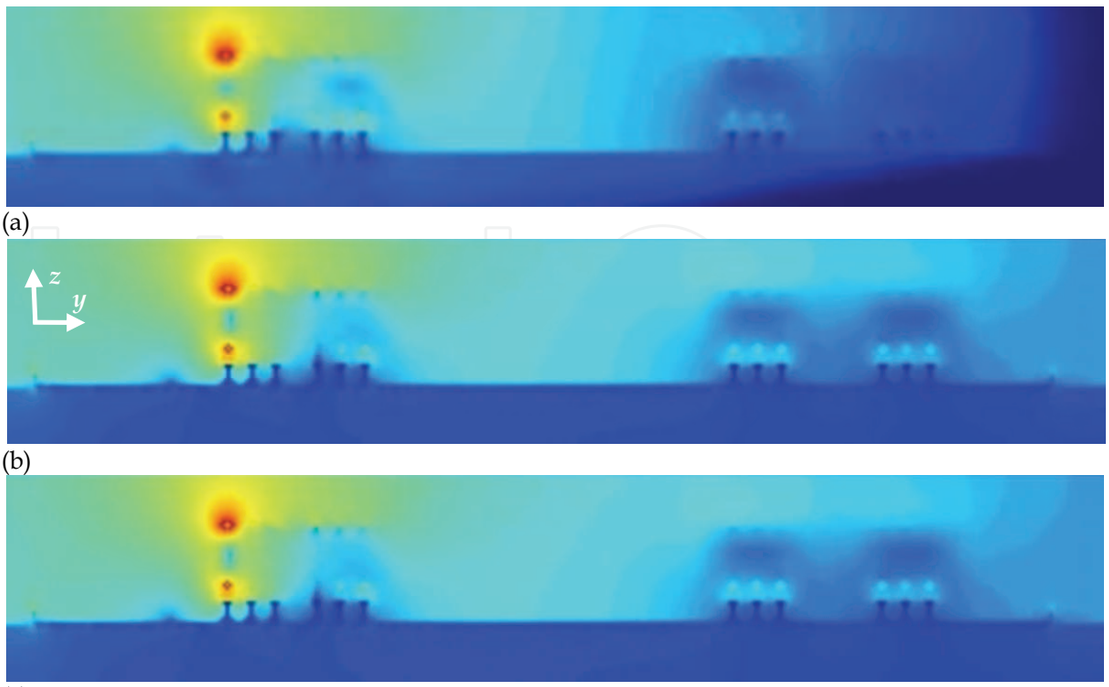


Fig. 16. Maximum induced voltages induced on transmission lines for (a) x = 370, (b) x = 347, (c) x = 316 and (d) x = 1173.

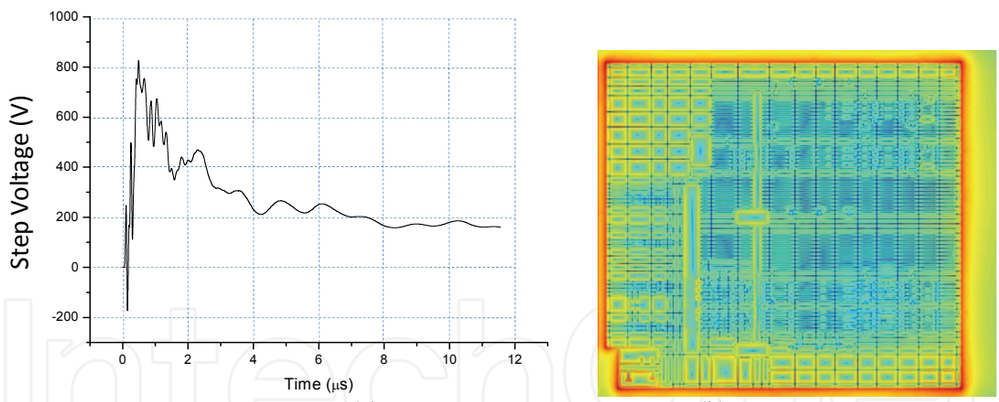


(a)

(b)

(c)

Fig. 17. Spatial electric field distribution for the plane parallel to the *yz*-plane which contains the discharge source, for: (a) t = 0.225 μs, (b) t = 0.365 μs and (c) t = 1.00 μs.



(a)

(b)

Fig. 18. (a) Step voltage as function of time and (b) E_z electric field component distribution for t = 38.5 μs at the plane of the ground grid.

4. Conclusion

This R&D project generated a computational environment for the analysis and synthesis of problems on EMC. The initially obtained results were consistent with those available in the literature and with the physics that the problems involve. The used methodology represents a full wave solution and can be used in any frequency range. The developed software can be used in a great range of different applications, as Maxwell's equations are solved by an automated parallel processing environment.

The association of the computational environment with the laboratory equipment acquired represents a desirable infra-structure for the realization of high level works.

Acknowledgements

This work was supported by ELETRONORTE – Centrais Elétricas do Norte do Brasil S/A and by the CNPq – Conselho Nacional de Desenvolvimento Cientifico e Tecnológico.

5. References

Ala, G., Buccheri, P. L., Romano, P., Viola, F. (2008). Finite Difference Time Domain Simulation of Earth Electrodes Soil Ionisation Under Lightning Surge Condition. S*cience, Measurement & Technology, IET,* Vol.2, No.3, May 2008, 134 - 145, ISSN: 1751-8822.

Baba, Y., Nagaoka, N. and Ametani, A. (2005). Modeling of thin wires in a lossy medium for FDTD simulations. *IEEE Transactions on Electromagnetic Compatibility,* Vol. 47, No. 1, Feb. 2005, pp. 54-60, ISSN: 0018-9375.

Hagan, M. T. & Menhaj, M. B. (1994). Training Feedforward Networks with the Marquardt Algorithm, *IEEE Transactions on Neural Networks,* Vol. 5, No. 6, Nov. 1994, 989–993, ISSN: 1045-9227.

Lazinica, A. (2009). *Particle Swarm Optimization,* InTech Education, ISBN: 978-953-7619-48-0.

Maloney, J. G. & Smith, G. S., R. (1992). The efficient modelling of thin material sheets in the finite-difference time-domain (FDTD) method. *IEEE Transactions on Antennas and Propagation,* Vol. 40, No. 3, March 1992, pp. 323-330, ISSN: 0018-926X.

Mattos, M. A. (2004). *Técnicas de Aterramento,* Okime, ISBN:8598294012, Brazil.

Oliveira, R. M. S. & Sobrinho, C. L. S. S. (2007), UPML Formulation for Truncating Conductive Media in Curvilinear Coordinates, *Numerical Algorithms*, vol. 46, No. 4, Dec. 2007, pp. 295-319, ISSN: 1572-9265.

Oliveira, R. M. S. & Sobrinho, C. L. S. S. (2009). Computational Environment for Simulating Lightning Strokes in a Power Substation by Finite-Difference Time-Domain Method. *IEEE Transactions on Electromagnetic Compatibility*, Vol. 51, No. 4, Vov. 2009, pp. 995-1000, ISSN: 0018-9375.

Rahmat-Sami, Y. & Michielsssen, E. (1999). *Electromagnetic Optimization by Genetic Algorithms,* John Wiley & Sons, ISBN: 0471295450, Canada.

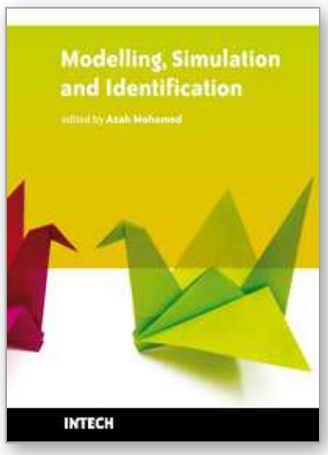
Taflove, A. & Hagness, S. C. (2005), *Computational Electrodynamics: The Finite-Difference Time-Domain Method*, Artech House, ISBN: 1580538320, Boston-London.

Tanabe. K. (2001). Novel method for analyzing the transient behavior of grounding systems based on the finite-difference time-domain method, *Proceedings of Power Engineering Society Winter Meeting*, pp. 1128-1132, OH USA, Feb. 2001, IEEE, Columbus.

Yee, K.(1996), Numerical solution of initial boundary value problems involving Maxwell´s equations in isotropic media, *IEEE Trans. Antennas and Propagation*, vol. 14, No. 3, May 1966, pp. 302-307, ISSN: 0018-926X.

IntechOpen

IntechOpen



Modelling, Simulation and Identification

Edited by Azah Mohamed

ISBN 978-953-307-136-7
Hard cover, 354 pages
Publisher Sciyo
Published online 18, August, 2010
Published in print edition August, 2010

Modeling, simulation and identification has been actively researched in solving practical engineering problems. This book presents the wide applications of modeling, simulation and identification in the fields of electrical engineering, mechanical engineering, civil engineering, computer science and information technology. The book consists of 17 chapters arranged in an order reflecting multidimensionality of applications related to power system, wireless communication, image and video processing, control systems, robotics, soil mechanics, road engineering, mechanical structures and workforce capacity planning. New techniques in signal processing, adaptive control, non-linear system identification, multi-agent simulation, eigenvalue analysis, risk assessment, modeling of dynamic systems, finite difference time domain modeling and visual feedback are also presented. We hope that readers will find the book useful and inspiring by examining the recent developments in the applications of modeling, simulation and identification.

How to reference

In order to correctly reference this scholarly work, feel free to copy and paste the following:

Rodrigo M.S de Oliveira, Reinaldo C. Leite, Ricardo H. Chamie Filho, Yuri C. Salame and Carlos Leonidas S.S. Sobrinho (2010). Applications of the Parallel-LN-FDTD Method to Calculating Transient EM Field in Complex Power Systems, Modelling, Simulation and Identification, Azah Mohamed (Ed.), ISBN: 978-953-307-136-7, InTech, Available from: http://www.intechopen.com/books/modelling--simulation-and-identification/techniques-and-methods-for-calculation-and-visualization-of-transient-electromagnetic-fields-interac

INTECH
open science | open minds

InTech Europe
University Campus STeP Ri
Slavka Krautzeka 83/A
51000 Rijeka, Croatia
Phone: +385 (51) 770 447
Fax: +385 (51) 686 166
www.intechopen.com

InTech China
Unit 405, Office Block, Hotel Equatorial Shanghai
No.65, Yan An Road (West), Shanghai, 200040, China
中国上海市延安西路65号上海国际贵都大饭店办公楼405单元
Phone: +86-21-62489820
Fax: +86-21-62489821

© 2010 The Author(s). Licensee IntechOpen. This chapter is distributed under the terms of the Creative Commons Attribution-NonCommercial-ShareAlike-3.0 License, which permits use, distribution and reproduction for non-commercial purposes, provided the original is properly cited and derivative works building on this content are distributed under the same license.

IntechOpen

IntechOpen